Elementary processes of antimicrobial peptide PGLa-induced pore formation in lipid bilayers

メタデータ	言語: eng
	出版者:
	公開日: 2019-05-07
	キーワード (Ja):
	キーワード (En):
	作成者: Parvez, Farliza, Alam, Jahangir Md., Dohra, Hideo, Yamazaki, Masahito
	メールアドレス:
	所属:
URL	http://hdl.handle.net/10297/00026432

Elementary Processes of Antimicrobial Peptide PGLa−Induced Pore Formation in Lipid Bilayers

Farliza Parvez,[a] Jahangir Md. Alam,[b,#] Hideo Dohra,[c] and Masahito Yamazaki[a, b, d,]*

[a] Integrated Bioscience Section, Graduate School of Science and Technology, Shizuoka University, Shizuoka, 422-8529, Japan

[b] Nanomaterials Research Division, Research Institute of Electronics, Shizuoka University, Shizuoka 422-8529, Japan

[c] Instrumental Research Support Office, Research Institute of Green Science and Technology,

[d] Department of Physics, Faculty of Science, Shizuoka University, Shizuoka 422-8529, Japan.

[#]Present address: Department of Biotechnology and Genetic Engineering, Islamic University, Kushtia-7003, Bangladesh

*Correspondence should be addressed to:

Dr. Masahito Yamazaki,

Nanomaterials Research Division, Research Institute of Electronics, Shizuoka University

836 Oya, Suruga-ku, Shizuoka 422-8529, Japan

TEL and FAX: 81-54-238-4741, Email: yamazaki.masahito@shizuoka.ac.jp

ABSTRACT

Antimicrobial peptide PGLa induces the leakage of intracellular content, leading to its bactericidal activity. However, the elementary process of PGLa-induced leakage remains poorly understood. Here, we examined the interaction of PGLa with lipid bilayers using the single giant unilamellar vesicle (GUV) method. We found that PGLa induced membrane permeation of calcein from GUVs comprised of dioleoylphosphatidylcholine (DOPC) and dioleoylphosphatidylglycerol (DOPG) and its rate increased with time to reach a steady value, indicating that PGLa induced pores in the bilayer. The binding of PGLa to the GUV membrane raised its fractional area change, δ. At high PGLa concentrations, the time course of δ showed a two-step increase; δ increased to a value, δ_1, which was constant for an extended period before increasing to another constant value, δ_2, that persisted until aspiration of the GUV. To reveal the distribution of PGLa, we investigated the interaction of a mixture of PGLa and carboxyfluorescein (CF) -labeled PGLa (CF-PGLa) with single GUVs. The change of the fluorescence intensity of the GUV rim, I, over time showed a two-step increase from a steady value, I_1, to another, I_2, concomitant with the entering of CF-PGLa into the lumen of the GUV prior to AF647 leakage. The simultaneous measurement of δ and I indicated that their time courses were virtually the same and the ratios (δ_2/δ_1 and I_2/I_1) were almost 2. These results indicated that CF-PGLa translocated across the bilayer before membrane permeation. Based on these results, the elementary processes of the PGLa-induced pore formation were discussed.

Key words: antimicrobial peptide, PGLa, pore formation, transmembrane movement, stretching, cell-penetration

1. INTRODUCTION

Various organisms including human produce antimicrobial peptides (AMPs) and antibacterial proteins to defend against bacteria and fungi [1-3]. It is considered that the target of most AMPs is plasma membranes of microbes and these AMPs cause damage to the membranes such as pore formation, yielding increased membrane permeability [1-4]. In contrast, some AMPs can make transmembrane movement across the plasma membrane of bacteria to enter the cytoplasm without damaging the plasma membrane, instead binding to DNA or other proteins within the cell [5,6]. Although several models for the mechanisms of AMP-caused damage of plasma membrane have been proposed [1.2], but the elementary processes of the action mode of most AMPs against plasma membranes and lipid bilayers are not well understood.

One noted source of AMPs is the granular gland in the skin of African clawed frog, *Xenopus laevis*. The major components of this gland's secretions include magainin 2, peptidyl-glycylleucine-carboxyamide (aka Peptide beginning with Glycine and ending with Leucine Amide, or PGLa), and xenopsin precursor [7,8]. All of these compounds are AMPs [9,10]. PGLa is composed of 21 amino acid residues (GMASKAGAI-AGKIAKVALKAL-NH2). Thus, PGLa is a positively charged peptide, containing four Lys (K) residues; this peptide can bind preferentially to the negatively charged outer leaflet of cytoplasmic membranes of bacteria cells using their electrostatic interaction [1]. The binding of PGLa to lipid bilayers has been investigated using various biophysical techniques [11-15]. Upon binding to a lipid bilayer, PGLa forms an α-helical structure in the monolayer interface and orients parallel to its surface (S-state) [13-15]; at higher concentrations of PGLa, the peptide assumes a tilted orientation (T-state) [14,15]. To reveal the cause of the bactericidal activity of PGLa, the interaction of the peptide with lipid bilayers previously was examined using large unilamellar vesicle (LUV) suspension method [16-19]. These studies indicated that PGLa causes leakage of water-soluble fluorescent dyes from LUV lumens, suggesting that PGLa forms pores in lipid bilayers. It was also reported that a mixture of PGLa and magainin 2 yielded enhanced (synergistic) leakage of internal contents [16,17,18,20], likely with related structural changes [21-23]. However, the elementary processes underlying PGLa-caused leakage of the internal contents and the synergism of pore formation induced by a mixture of PGLa and magainin 2 remained

unclear, because the LUV suspension method can provide only ensemble-average values of the physical quantities of many LUVs in a suspension, despite the fact that individual LUVs were at various stages of the process [24].

In contrast, giant unilamellar vesicles (GUVs) of lipid bilayers, i.e., lipid vesicles with diameters greater than 10 μm, can be observed using optical microscopy, and hence the shapes of GUVs and the localization of fluorescent probes in GUV membranes have been investigated [25-28]. Recently the single GUV method has been developed for investigation of the interaction of peptides/proteins with lipid bilayers [24,29]. In this method, we measure the change of the structure and physical quantities of an individual GUV over time during its interactions with peptides/proteins, and then we perform the same experiments using many "individual GUVs". Finally, we analyze the results of many individual GUVs statistically to obtain kinetic constants for their elementary processes. Using this method, we can obtain knowledge on the processes of AMP-induced pore formation (e.g., the rate constants both of pore formation and of leakage through these pores) [30-32], and those of entering of cell-penetrating peptides (CPPs) into the lumen of GUVs [33,34]. The single GUV method can be used to examine the relationships among localization of peptides in GUV membranes and pore formation, and to assess the effects of tension on peptide-caused pore formation [34-36]. These results could not be obtained using the LUV suspension method, demonstrating the advantage of the single GUV method [24,29].

In the work described here, we examined the processes of PGLa-caused leakage of internal contents in an effort to define the mechanism of this leakage. Specifically, we used the single GUV method to determine the interactions of PGLa with lipid membranes. In a first set of experiments, we investigated PGLa-induced leakage of a water-soluble fluorescent dye, calcein, from GUVs composed of dioleoylphosphatidylglycerol (DOPG)/dioleoylphosphatidylcholine (DOPC). The results directly indicated that PGLa caused pore formation in the GUV membranes. In a second set of experiments, to discover the mechanism of PGLa-caused pore formation, we examined the PGLa-caused change in the membrane area using the micropipette aspiration method. On the other hand, elucidation of the location of peptides in the GUV membranes during the interaction of peptides with single GUVs would provide us important information to discover the mechanism of peptide-

caused pore formation [35]. Therefore, in a third set of experiments, we examined the interaction of PGLa attached with a fluorescent dye, carboxyfluorescein (CF-PGLa) with individual GUVs containing a water-soluble fluorescein dye, Alexa Fluor 647 hydrazide (AF647) using confocal laser-scanning microscopy (CLSM) [33-35]. Based on these results, the processes of PGLa-caused pore formation and entering of PGLa into the lumen were discussed.

2. MATERIALS AND METHODS

2.1. Chemicals

DOPG and DOPC were bought from Avanti Polar Lipids, Inc. (Alabaster, AL). AF647, and 5-(and 6)-carboxyfluorescein (CF) succinimidylester were bought from Invitrogen, Inc. (Carlsbad, CA). Calcein was bought from Dojindo Laboratory (Kumamoto, Japan). Bovine serum albumin (BSA) was bought from Wako Pure Chemical Industry, Ltd. (Osaka, Japan). PGLa was synthesized and purified using the same method described previously [30]. CF-labeled PGLa (i.e., CF-PGLa) with one fluorophore CF at the N-terminus of the peptide was prepared using the same method [33] by the reaction of CF succinimidylester (30 mg) with PGLa-peptide resin (74 mg) (molar ratio of reagent to peptide: 3 to 1) in dimethylformamide for 24 h at room temperature. The methods for cleavage and purification of the peptide were the same as described in refs. [30,35]. The method for liquid chromatography−mass spectrometry (LC−MS) analysis for PGLa and CF-PGLa was described previously [6]. The measured masses of PGLa and CF-PGLa were 1967.18 ± 0.01 and 2325.25 ± 0.01 Da, respectively, which agreed with the molecular masses based on the monoisotopic mass of all of the atoms. CF-PGLa concentrations in a buffer were determined by measuring absorbance at 492 nm and using the molar absorption coefficient of CF (81, 000).

2.2. Preparation and observation of GUVs

DOPG/DOPC (4/6, molar ratio)-GUVs (hereafter PG/PC (4/6)-GUVs) were prepared in buffer A (10 mM PIPES, pH 7.0, 150 mM NaCl, and 1 mM EGTA) containing 0.10 M sucrose and 6 μM AF647 (or 1 mM calcein) by the natural swelling method [35], and were purified in buffer A containing 0.10 M glucose using the

membrane filtering method [37]. Following purification, an aliquot (~300 μL) of the GUV suspension was transferred into hand-made micro-chambers which were coated by BSA [35].

2.3. Measurement of fractional change in the membrane area induced by binding of PGLa to the membrane

We measured the area change of PG/PC (4/6)-GUVs induced by the interaction of PGLa using the micropipette aspiration method under an inverted differential interference contrast (DIC) microscope (IX-71, Olympus, Tokyo, Japan) at 25 ± 1 °C controlled by a stage thermocontrol system (Thermoplate, Tokai Hit, Shizuoka, Japan) [26,35,36]. We described the method briefly as follows (see the details in the ref. [35]). First, we held a GUV by aspiration of micropipette A (its membrane tension, σ, was adjusted to be 0.50 mN/m) for 2 min to eliminate the problem of the hidden area [26,35]. σ was controlled by aspiration pressure, ΔP, which is the pressure difference between the outside and the inside of the micropipette A as follows [26].

$$\sigma = \frac{\Delta P d_P}{4(1 - d_P/D_V)} \tag{1}$$

where d_p is the internal diameter of the micropipette and D_v is the diameter of the spherical cap segment (on the outside of the micropipette) of the aspirated GUV. Then, we added a PGLa solution continuously from another micropipette (micropipette B) into the neighborhood of the GUV. The distance between the GUV and the tip of micropipette B was ~40 μm, and the ΔP of micropipette B was −30 Pa [35]. The fractional change in the area of the GUV membrane as a function of time (t) after starting interaction with PGLa, $\delta(t)$, can be expressed as $\delta(t) = \Delta A(t)/A_0$, where A_0 is the area of a GUV before the interaction with PGLa and $\Delta A(t)$ is the change in the area of the GUV membrane at time (t) after starting interaction with PGLa. The change in $\delta(t)$ over time is mainly determined by the change in the projection length, $\Delta L(t)$ ($= L(t) - L_0$, where $L(t)$ and L_0 are the projection lengths of the GUV at time (t) after and before the interaction with PGLa, respectively). The equation for $\delta(t)$, assuming constant volume, is given by the following equation [26]:

$$\delta(t) = \frac{\Delta A(t)}{A_0} = \frac{d_P \Delta L(t)(1 - d_P/D_V)}{D_{V0}^2} \tag{2}$$

where D_v and D_{v0} are the D_v after and before the interaction with PGLa, respectively.

6

2.4. Measurement of PGLa-caused leakage of calcein from individual GUVs

Interaction of PGLa with single PG/PC (4/6)-GUVs containing calcein in their lumens were performed under an inverted fluorescence, phase-contrast microscope (IX-70. Olympus) with three neutral density filters and an EM-CCD camera (C9100-12, Hamamatsu Photonics K.K., Hamamatsu, Japan) at 25 ± 1 °C controlled by a stage thermocontrol system (Thermoplate, Tokai Hit) [31]. In each experiment, we added continuously a specific concentration of PGLa in buffer A containing 0.1 M glucose to the vicinity of a GUV through a 20-μm-diameter glass micropipette whose position was controlled by a micromanipulator. The distance between the GUV and the tip of the micropipette was ~70 μm. The ΔP of micropipette was -30 Pa. The details of this method are described in our previous reports [24,35]. PGLa concentrations in the vicinity of the GUV were determined by the method described in our previous paper [35], which was described briefly in the Supporting Information (SI). The fluorescence intensity (FI) of a GUV lumen due to calcein was determined using an AquaCosmos (Hamamatsu Photonics K.K.).

2.5. Investigation of the interactions of CF-PGLa/PGLa with individual GUVs using CLSM

Here we used a confocal laser scanning microscope (FV1000-D, Olympus) with 60× objective at 25 ± 1 °C controlled by a stage thermocontrol system (Thermoplate, Tokai Hit) [33-35]. For CLSM measurements, fluorescence images due to AF647 (excited by a laser at $\lambda = 635$ nm) and of CF-PGLa (excited by a laser at $\lambda = 473$ nm), along with DIC images, were obtained using a 60× objective (UPLSAPO060X0, Olympus) (numerical aperture = 1.35) [33-35]. To examine the interaction of CF-PGLa/PGLa with single GUVs containing AF647 in their lumens, various concentrations of CF-PGLa/PGLa solution in buffer A containing 0.10 M glucose were provided successively near the GUV by a glass micropipette (20 μm diameter) whose position was controlled by a micromanipulator. The separation between the GUV and the tip of the micropipette was 50 μm and the ΔP was -30 Pa. The details of these methods were reported in refs. [33-35]. PGLa concentrations near single GUVs were determined by the method reported in ref. [35], which was described briefly in the SI.

To measure the change of the FI (over time) of a GUV lumen due to AF647 and due to CF-PGLa/PGLa, a small circle ~50% of the diameter of the GUV at the center of the GUV lumen (so that the small circle did not

include the GUV rim during the interaction with CF-PGLa/PGLa) was specified, and then the FI of this area was measured as a function of time, then this intensity was corrected by subtracting the background intensity (i.e., the FI of the same buffer). To measure the change of the FI (over time) of the GUV membrane due to CF-PGLa/PGLa (i.e., the rim intensity), we applied the similar method reported in ref. [35] using 6 lines from the center of each GUV image to its outside. We defined the edge of the GUV, where the FI due to AF647 in the GUV lumen greatly decreased, as the rim of the GUV. We always observed a sharp, large peak at the edge of the GUV, which was defined as the rim intensity. We obtained the mean values and the standard deviations of 6 rim intensities at 5−20 s intervals, and indicate these data in Fig. 3 and Fig. 4.

2.6. Simultaneous measurement of the time course of CF-PGLA/PGLa-induced change in the membrane area, CF-PGLa concentration in the membrane, and leakage of AF647.

We used a confocal laser scanning microscope at 25 ± 1 °C with a stage thermocontrol system [23]. First, a single PG/PC (4/6)-GUV containing AF647 was held at the tip of micropipette A (~10-μm-diameter) by aspiration (so that the membrane tension was 0.50 mN/m) for 2 min. Next, CF-PGLa/PGLa solution was successively provided from another micropipette B (~20-μm-diameter) near the GUV. PGLa concentrations near single GUVs were determined by the method reported in ref. [35] , which was described briefly in the SI. The distance between the GUV and the tip of micropipette B was ~40 μm. The measurement method for the fractional change in membrane area, $\delta(t) = \Delta A(t)/A_0$, was described in Section 2.3. The FI of the rim of the GUV was measured as described in Section 2.5.


3. RESULTS AND DISCUSSION

3.1. PGLa-induced leakage of calcein in individual PG/PC (4/6)-GUVs

We investigated the interaction of PGLa with single PG/PC (4/6)-GUVs under fluorescence, phase-contrast microscope at 25 °C. The GUV lumens contained calcein (water-soluble fluorescent probe) in buffer A containing 0.10 M sucrose, and the aqueous solution in the outside of the GUVs was buffer A containing 0.10 M glucose. Figure 1A shows microscopic images of a GUV interacting with 19 μM PGLa. Before the interaction

8

of PGLa, the phase-contrast microscopic image of the GUV (Fig. 1A (1)) had a high contrast because of the

concentration difference of sucrose and glucose between the GUV lumen (0.10 M sucrose) and the outside of

the GUV (0.10 M glucose) (producing the difference in refractive index). The first image ($t = 0$) in Fig. 1A (2)

shows that the same GUV had a high fluorescence intensity (FI) due to calcein in its lumen, indicating a high

concentration of calcein in the GUV lumen. During the interaction of the PGLa solution, the FI of the GUV

lumen did not change significantly until 115 s, following which the FI decreased with time (Fig. 1A (2)). Since

Figure 1

(A)

(B) (C)

(D) (E)
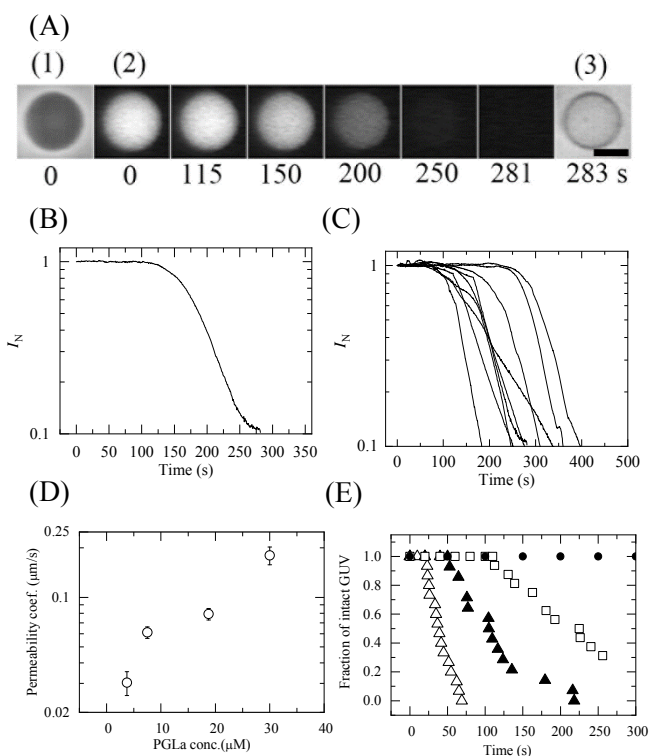
Figure 1. Calcein leakage from individual PG/PC (4/6)-GUVs caused by PGLa. (A) Microscopic images of a GUV interacting with 19 µM PGLa. (1) (3) Phase-contrast images of the GUV. (2) Fluorescence images of the GUV. The numerals below each image indicate the time of the interaction of PGLa with the GUV. The bar: 20 µm. (B) The change in $I_N(t)$ of the GUV lumen due to calcein over time, which corresponds to the result of (A). (C) Other time courses of the change in $I_N(t)$ of individual GUVs during the interaction of 19 µM PGLa. Each curve shows the result for each GUV. (D) Dependence of the steady value of membrane permeability coefficient of calcein P^s on PGLa concentration. (E) Change of P_{intact} of GUVs over time in the interaction of (Δ) 30, (▲) 19, (□) 3.8, and (●) 1.5 µM PGLa.

9

the FI of the GUV lumen is proportional to the calcein concentration there, the decrease in FI indicates the decrease in calcein concentration in the lumen. Figure 1B shows a semi-log plot of the normalized FI of the GUV lumen, $I_N(t)$ ($= I(t)/I(0)$), vs. time (s), where $I(t)$ and $I(0)$ are the FI of the GUV lumen at time t, and that of the intact GUV before the interaction of PGLa, respectively. The rate of the change in $I_N(t)$ (i.e., the absolute value of the slope of the curve) initially remained zero up to 115 s and grew with time to reach a maximum rate at 160 s, which subsequently remained constant up to 240 s. When $I_N(t)$ became less than 0.1, a phase-contrast image of the same GUV (Fig. 1A (3)) shows that the GUV structure did not change greatly nor exhibit detectable breaks. During the leakage, the association of GUVs, their membrane fusion, and large shape changes did not occur. These results indicate that PGLa-induced pores in the bilayer through which the calcein leakage occurred from the GUV lumen to its outside [30-32,38]. Thus, the time of the start of the decrease in FI can be considered as the time of the start of pore formation in the lipid bilayer. Furthermore, a large reduction in the phase-contrast of the GUV (Figs. 1A (1) and (3)) indicates that sucrose and glucose also permeated through the same pores. Comparison of the same leakage experiments performed using 27 individual GUVs indicated that calcein leakage began randomly and that the change of $I_N(t)$ of each GUV over time after the leakage began was essentially the same, such that the rate of the reduction in $I_N(t)$ remained zero for an extended interval (50−220 s depending on GUVs) and grew with time to reach a maximum value (Fig. 1C).

This result directly indicated that pore formation started randomly and that the rate of leakage (i.e., membrane permeation) remained zero for an extended interval and grew with time to reach a maximum value. The slope of the reducing curves in Fig. 1C is proportional to the membrane permeability coefficient of calcein per unit area of a GUV membrane, $P(t)$ (m/s) [38]. Thus, the result of Fig. 1C indicates that after the leakage began the value of P grew with time before reaching a maximum value, P^s, which continued for an extended time (80 s) until P value reduced. This time course of membrane permeation of calcein is similar to that of lysenin [38], but different from that of magainin 2 (i.e., in the magainin 2-induced membrane permeation, at the initial time after starting the membrane permeation the value of P was large, but it subsequently decreased to reach a final, steady value [32]). There are two possible sources for the increase in $P(t)$: a growth in size of pore,

or a growth in number of pores with the same size. The mean value and standard deviation (SD) of P^s was (7.9 $\pm$ 0.6) $\times$ 10^{-2} μm/s ($n = 27$) with 19 μM PGLa. Figure 1D indicates that P^s was raised as PGLa concentration increased.

Next, we analyzed PGLa-caused pore formation more quantitatively. For estimation of the rate of pore formation, it is indispensable to examine the change of the fraction of intact GUV over time (i.e., GUVs with no leakage of calcein), $P_{intact}(t)$, among all examined GUVs [30,31]. Generally, when the rate of decrease in $P_{intact}(t)$ is large, the speed of pore formation is large. Figure 1E shows the change of P_{intact} of PG/PC (4/6)-GUVs over time, indicating that the rate of decrease in $P_{intact}(t)$ was raised as PGLa concentration increased from 3.8 to 30 μM. At PGLa concentrations not exceeding 1.5 μM (including 0 μM, i.e., buffer A containing 0.1 M glucose), no pore formation occurred in any of the GUVs for 6 min. These results indicated that the rate of PGLa-caused pore formation in the bilayer was raised as PGLa concentration increased. In the case of magainin 2, we proposed the two-state transition model from the intact state (i.e., the state before leakage) to the pore state, and thereby a change of the P_{intact} of GUVs over time was well-fitted by a single exponential function, providing the rate constant of the two-state transition. This two-state transition model for the initial stage of magainin 2-caused pore formation has been proved recently [35,36]. In contrast, in the case of PGLa, the intact state is composed of at least two states (see the details later), which is greatly different from that of magainin 2. Therefore, we could not determine the rate constant of PGLa-caused pore formation.

3.2. PGLa-induced expansion of membrane area

We examined the effects of the binding of PGLa to the membranes of single PG/PC (4/6)-GUVs on the area of these membranes using the method described previously [35]. Figure 2A indicates that, in the interaction of 1.2 μM PGLa with a GUV, the fractional expansion in the membrane area, δ, grew over time to reach a constant value in less than 50 s. The mean value and SD of the steady value of δ was 0.028 $\pm$ 0.001 ($n = 10$). At higher concentrations of PGLa (i.e., those capable of inducing pore formation), a two-step increase in δ was observed. Figure 2B shows that in the interaction of 5.8 μM PGLa with a GUV. For example, in a GUV (red ○ in Fig. 2B),

δ rapidly grew to a first, constant value, δ_1, at $t = 36$ s, then was constant until $t = 156$ s, at which point the δ again began to grow and, after 80 s, reached another constant value, δ_2 (i.e., a two-step increase in δ). Then, at 330 s the GUV disappeared suddenly by aspiration into the micropipette. As we discussed in our previous paper, this aspiration is due to rupture of the GUV after pore formation [35]. At 5.8 μM PGLa, all the examined GUVs were aspirated within 6 min ($n = 18$ in 2 independent experiments). In 10 GUVs, we observed the two-step increase in δ, and the mean values and SDs of δ_2/δ_1 was 1.9 ± 0.2 ($n = 10$). But in other 8 GUVs, we observed that GUVs were aspirated into the micropipette before reaching another steady value, δ_2. In the interaction of 2.9 μM PGLa with a GUV, a two-step increase in δ was observed in 8 GUVs and the mean values and SDs of δ_2/δ_1 was 1.8 ± 0.1 ($n = 8$), but only a one-step increase was observed within 6 min in other 12 GUVs (Fig. 2C). The value of δ at the 1st steady state, δ_1, was raised as PGLa concentration increased, but at and above 1.2 μM PGLa, δ_1 became essentially constant ($= 0.029 \pm 0.002$) (Fig. 2D).

Figure 2
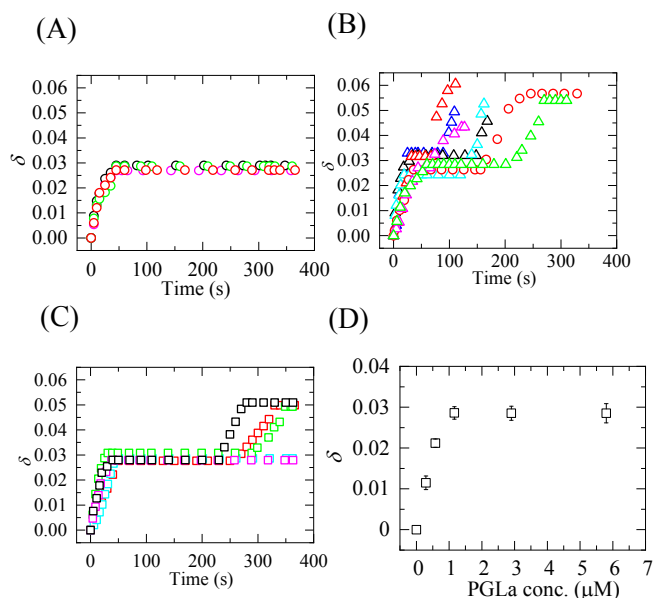

Figure 2. PGLa-caused expansion of the membrane area. Change of the fractional expansion in area, δ, of single GUVs over time after starting interaction with 1.2 μM (A), 5.8 μM (B), and 2.9 μM PGLa (C). Each curve shows the result for each GUV. (D) Dependence of the δ at the 1st steady state, δ_1, on the PGLa concentration in buffer A. The mean values and the SD of δ_1 ($n = 10$–20) for each PGLa concentration are shown.

3.3. Relationship between the distribution of PGLa in a GUV and the AF647 leakage

To elucidate the mechanism of PGLa-caused pore formation in the bilayers, the knowledge of distribution of PGLa in a GUV is indispensable. To reveal the connection between the distribution of PGLa in a GUV and pore formation, we used CLSM to examine the interaction of CF-PGLa/PGLa with individual PG/PC (4/6)-GUVs containing AF647. To monitor the location of PGLa here, we included a low concentration of the fluorescent probe-labeled PGLa (CF-PGLa) into higher concentration of PGLa [35], because generally fluorescent probe-labeled peptides behave in a little different way from the non-labeled peptides due to the attached hydrophobic fluorescent probes [33,34]. Figure 3A shows a CLSM image of a single GUV interacting with 19 μM CF-PGLa/PGLa (containing 0.15 μM CF-PGLa). Fig. 3A (1) shows that during the interaction of the CF-PGLa/PGLa solution the FI of the GUV lumen due to AF647 did not change significantly until 126 s, and subsequently the FI gradually diminished (Fig. 3A (1) & red line in Fig. 3B). As discussed in the previous section (regarding Fig. 1), the reduction in FI resulted from the leakage of AF647 from the lumen through the pores caused by PGLa. Thus, the time of start of decrease in FI (t = 126 s) corresponded to the time of start of AF647 leakage. This observation indicated that PGLa induced formation of pores in the bilayer (through which AF647 leaked out) at 126 s. The rate of leakage of AF647 was smaller than that of calcein (Fig. 1), probably because the size of AF647 (its Stokes-Einstein radius, R_{SE}, is ~0.9 nm based on the size (0.88 nm) of the similar compound, AF647 succinimidyl ester [39]) is larger than that of calcein [32] (R_{SE} = 0.74 nm). On the other hand, Fig. 3A (2) shows that the FI of the GUV rim (i.e., the rim intensity, I) due to CF-PGLa rapidly grew to a value, I_1, at around t = 31 s, then was constant until t = 70 s (green square in Fig. 3B). This result indicated that the binding of CF-PGLa/PGLa to the GUV membrane grew with time to reach a value at 31 s and then the CF-PGLa/PGLa concentration in the membrane was constant for 40 s. At t = 70 s, the I restarted to grow and then reached another constant value, I_2, at around 91 s. The I_2 did not change after the start of pore formation. Similar results, including a two-step increase in I, were observed for other GUVs (n = 8). The I rapidly grew to a value, I_1 (the rim intensity of the first steady state), at ~30 s, then was constant for an extended time (25-70 s). Then, the I again increased before reaching another constant value, I_2 (the rim intensity of the second steady state).

13

Figure 3

(A)

(B)

(C)

(D)
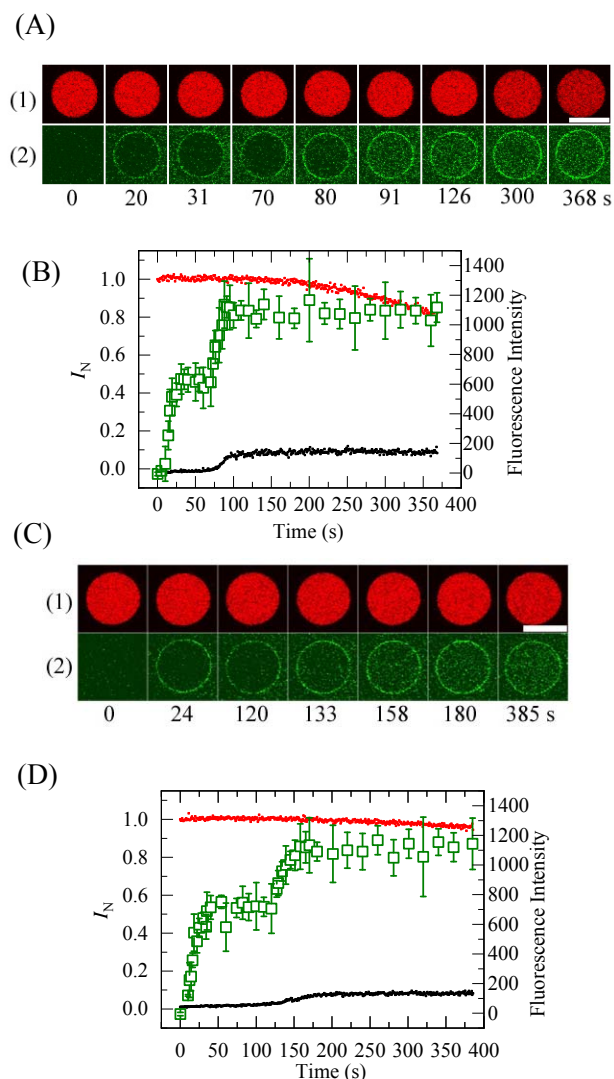
Figure 3. CF-PGLa/PGLa-induced AF647 leakage and distribution of CF-PGLa in single PG/PC (4/6)-GUVs. (A) Interaction of 19 µM CF-PGLa/PGLa (containing 0.15 µM CF-PGLa) with a GUV. CLSM images due to (1) AF647 and (2) CF-PGLa. The numerals below each image indicate the time of interaction of CF-PGLa/PGLa with the GUV. The bar: 20 µm. (B) Change in FI of the GUV shown in (A) over time. The solid red line denotes to the FI of the GUV lumen due to AF647, expressed as normalized FI (left axis), $I_N(t)$. The green open squares denote to the FI of CF-PGLa in the rim of the GUV (right axis), and the mean values and the SD are shown. The solid black line corresponds to I_{lumen} due to CF-PGLa (right axis). (C) Interaction of 3.8 µM CF-PGLa/PGLa (containing 0.15 µM CF-PGLa) with a GUV. CLSM images due to (1) AF647 and (2) CF-PGLa. The numerals below each image indicate the time of the interaction of CF-PGLa/PGLa with the GUV. The bar: 20 µm. (D) Change in FI of the GUV shown in (C) over time. The symbols are the same in the panel (B). .

After an extended period, pore formation began. The I_2 did not change after the start of AF647 leakage. The mean values and SDs of I_2/I_1 was 1.8 ± 0.4 ($n = 8$). The mean lag time between the time when the I reached the second constant value I_2 and the time when the leakage started, t_P, was 45 ± 9 s ($n = 8$). We also analyzed the FI of the lumen due to CF-PGLa, I_{lumen} (Fig. 3A2). I_{lumen} began to increase rapidly at around $t = 73$ s, then reached a maximum at 95 s; the I_{lumen} did not change further after pore formation (black solid line in Fig. 3B). The mean value of this maximum of I_{lumen} was 180 ± 20 ($n = 9$), which was a little larger that the FI of the aqueous solution in the vicinity of the GUV (outside the GUV) (140 ± 10, $n = 9$). This may be owing to the existence of small vesicles in the lumen of the GUVs, because the FI of CF-PGLa increased after it binds to the membrane. The starting time of the increase in I_{lumen} was essentially the same as that when the I started to increase from I_1 to I_2. We made the same experiment presented in Fig. 3A using different CF-PGLa/PGLa concentrations. Figure 3C shows the result with 3.8 µM CF-PGLa/PGLa (containing 0.15 µM CF-PGLa). The AF647 leakage began at 182 s (red line in Fig. 3D). The I quickly grew to a value, I_1, at around $t = 35$ s, then was constant for ~90 s, and at $t = 127$ s, the I restarted to grow to another constant value, I_2 (green square in Fig. 3D). We observed such a two-step increase in I in 5 GUVs among all GUVs ($n = 11$); the mean values and SDs of I_2/I_1 was 1.6 ± 0.3 ($n = 5$) and that of t_P was 42 ± 9 s ($n = 5$). In other 6 GUVs, the I rapidly grew to a value, I_1, at ~50 s, then was constant for an extended time and the AF647 leakage did not occur until the end of measurement (~ 400 s) (e.g., Fig. S1 in the SI). The mean value of I_1 for 3.8 µM CF-PGLa/PGLa (containing 0.15 µM CF-PGLa) was 720 ± 20 ($n = 11$) was almost similar to that of I_1 for 19 µM CF-PGLa/PGLa (containing 0.15 µM CF-PGLa) (= 660 ± 40 ($n = 8$)), indicating that the binding constant of CF-PGLa to PG/PC (4/6)-GUVs was much larger than that of PGLa. This result may explain that the rate of CF-PGLa-induced pore formation and that of CF-PGLa-induced leakage of AF647 were larger than those induced by PGLa (see the details later).

We postulated that I is proportional to the CF-PGLa concentration in a GUV membrane, C_M, under the condition that the concentration is so low that no significant energy transfer occurs between CF-PGLa molecules [34]. Hence, the time course of I during the interaction of CF-PGLa with individual GUVs (Fig. 3B and 3D) indicated that C_M rapidly increased to a steady value, C_M (S1), then was constant for an extended time, until C_M

suddenly restarted to grow and reached another steady value, C_M (S2). Here we designate the state that has a steady value C_M (S1) as state A, and the state that has a steady value C_M (S2) as state B. Pore formation (i.e., the AF647 leakage) started at ~50 s (= t_P) after C_M reached the second steady value (i.e., when the GUV achieved state B). If C_M remained at the first steady state corresponding to state A, membrane permeation did not occur. After membrane permeation of AF647, C_M did not increase further, which suggested that the CF-PGLa concentration in the inner monolayer has already achieved saturation before membrane permeation. These results indicated that CF-PGLa initially was distributed only in the outer leaflet, then translocated into the inner leaflet before the start of leakage and simultaneously CF-PGLa binds with the outer leaflet from the aqueous solution because the rate of binding of CF-PGLa to the membrane is large, until the CF-PGLa concentration in the inner leaflet became the same as that in the outer one. This state continued for a long time, even after membrane permeation. Moreover, I_{lumen} due to CF-PGLa started to increase rapidly when C_M began to grow from the first constant value, C_M (S1), indicating that entering of CF-PGLa into the lumen began at this time. This result indicated that CF-PGLa started to enter the GUV lumen immediately after CF-PGLa translocates into the inner monolayer.

We also investigated the interaction of 100% CF-PGLa with single PG/PC (4/6)-GUVs containing AF647 using CLSM (in the section S.2. and Fig. S2 in the SI). We obtained similar results to those shown in Fig. 3, although the rate of CF-PGLa-induced pore formation and that of CF-PGLa-induced leakage of AF647 were larger than that induced by PGLa.

3.4. Relationship of CF-PGLa/PGLa-induced expansion of the area of GUV membrane, CF-PGLa/PGLa concentration in the membrane, and AF647 leakage

Concurrently, we measured the CF-PGLa/PGLa-induced expansion of the membrane area (δ), the growth in rim intensity due to CF-PGLa (I), and the lumen intensity due to AF647. Figure 4A shows the CLSM images of a GUV interacting with 2.9 μM CF-PGLa/PGLa, where pore formation occurred at less than 6 min. The analysis of Fig. 4A indicates that both the δ and the I of the GUV rapidly grew to steady values of δ_1 and I_1,

respectively, within 60 s, and then were constant for an extended time (~175 s) (Fig. 4B). Then, at 240 s, both the δ and the I started to increase rapidly until new steady values of δ_2 and I_2, respectively, were achieved; these values remained constant until disappearance of the GUV by aspiration into the micropipette (due to pore formation) at 386 s. Thus, a two-step increase was observed in δ and I. The patterns of these time courses of δ and I were virtually the same. This observation supports the relationship $\delta \propto C_M$. The mean values and SDs of δ_2/δ_1 and I_2/I_1 were 1.9 ± 0.1 and 1.8 ± 0.3 ($n = 9$ for 2 independent experiments). Under the same conditions (2.9 μM PGLa), pore formation was not observed in several ($n = 10$) GUVs, and both the δ and the I rapidly increased to steady values of δ_1 and I_1 within 50 s, respectively, subsequently remaining constant until the end

Figure 4
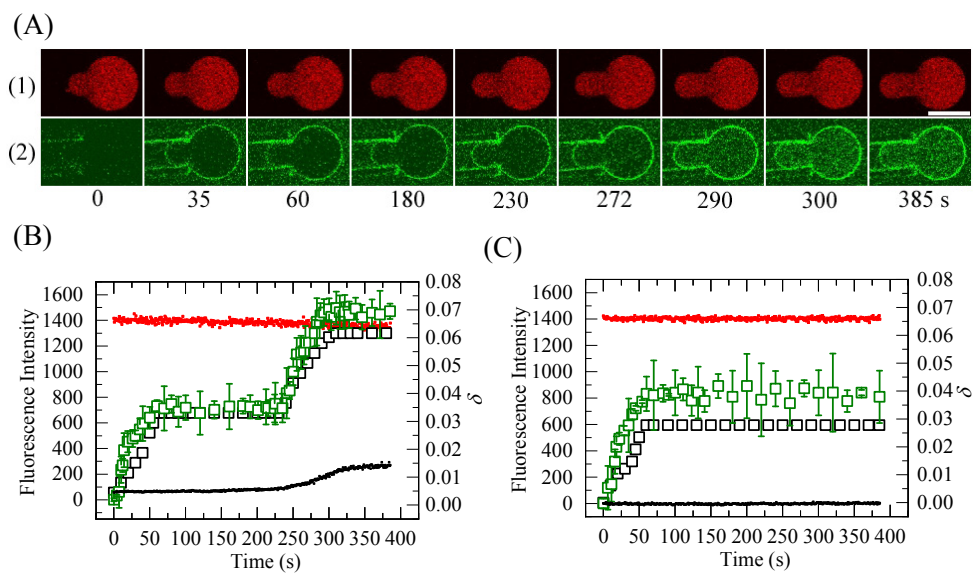
Figure 4. Time course of CF-PGLa/PGLa-induced change in δ, rim intensity and lumen intensity due to CF-PGLa, and the AF647 leakage in single PG/PC (4/6)-GUVs held at the tip of a micropipette. (A) CLSM images due to (1) AF647 and (2) CF-PGLa. A GUV held at the tip of a micropipette was interacted with 2.9 μM CF-PGLa/PGLa. The numerals below each image indicate the time of the initiation of CF-PGLa/PGLa with the GUV. The bar: 20 μm. (B) Change in FI of the GUV and δ of GUV shown in (A) over time. Red line denotes the FI of the GUV lumen due to AF647 (left axis). Black open squares denote δ (right axis). Green open squares represent the rim intensity due to CF-PGLa (left axis), and its mean values and the SD are shown. The solid black line corresponds to I_{lumen} due to CF-PGLa (left axis). (C) Change in FI and δ of another GUV under the same conditions as the panel (A). The symbols are the same in the panel (B). .

of the measurement (6 min) (i.e., demonstrating a one-step increase in δ and I) (Fig. 4C). In the case of 5.8 μM CF-PGLa/PGLa, the two-step increase in δ and I and subsequent pore formation were observed in all the examined GUVs. The mean values and SDs of δ_2/δ_1 and I_2/I_1 were 2.2 ± 0.1 and 1.8 ± 0.3 (n = 10 for 2 independent experiments), respectively.

4. GENERAL DISCUSSION

The results of Fig. 1 clearly indicated that PGLa caused pore formation in PG/PC (4/6) membranes, through which calcein leaked from the lumen to the outside. The pores were formed stochastically. The rate of PGLa-caused pore formation was raised as PGLa concentration in aqueous solution increased. Moreover, by analyzing the change of the leakage of calcein over time, the membrane permeability coefficient of calcein ($P(t)$) was obtained. $P(t)$ increased gradually with time to reach a steady, maximum value (i.e., the steady state of membrane permeation through the PGLa-induced pores), which continued for an extended time.. This time course of membrane permeation of calcein was similar to that observed for lysenin [38], but differed from that of magainin 2 [32]. These results indicate that PGLa forms pores in the bilayer for an extended time (e.g., more than 2 min for 19 μM in PG/PC (4/6)-membranes).

The results of Fig. 2 showed that at higher PGLa concentrations the two-step increase in δ was observed and the mean value of δ_2/δ_1 was 1.9 ± 0.2. There are two possible interpretations. One of the interpretation (interpretation A) is the structural change of PGLa in the lipid bilayer. PGLa forms structure A at lower concentrations, and it converts into structure B at higher concentration, which takes significant time (50 −300 s), depending on its condition. In this interpretation A, we have to assume that the fractional area change in the lipid bilayer induced by structure B is almost two-folds larger than that induced by structure A. Moreover, we have to consider that at 5.8 μM PGLa the aspiration of a GUV (due to pore formation) occurred before complete conversion to structure B in almost half of the examined GUVs. The results of NMR spectroscopy indicated that PGLa has only two structures in the lipid bilayers in the liquid-crystalline (L_α) phase; one is an α-helical structure at the monolayer interface, parallel to its surface (i.e., S-state) at low PGLa concentration, and the

18

other is a tilted orientation (i.e., T-sate) at higher PGLa concentrations [13-15]. One may infer that structure A corresponds to the S-state and structure B corresponds to the T-state. In the T-state, PGLa inserts into the hydrophobic core of the bilayer, and hence, the increase in area of the membrane due to the interaction of PGLa at the T-state is larger than that at the S-state, although we do not know that the fractional area change in the lipid bilayer induced by the T-state is almost two-folds larger than that induced by the S-state. In this interpretation A, PGLa locates only in the outer leaflet as the S-state or the T-state before pore formation. Another interpretation (interpretation B) is the change in location of PGLa in the GUV membrane; PGLa locates only in the outer leaflet at lower concentrations (i.e., asymmetric transbilayer distribution of PGLa), and it translocates across the bilayer and as a result PGLa locates in both leaflets at higher concentration (i.e., symmetric transbilayer distribution of PGLa). It takes significant time (50−300 s) for the translocation, depending on its condition. One may reasonably infer that the fractional area change in the lipid bilayer induced by the symmetric transbilayer distribution is almost two-folds larger than that induced by the asymmetric transbilayer distribution (see the details in the later discussion). However, in the interpretation B, we assume that the structural change of PGLa (from A to B) does not induce the area change of the membrane.

The results in Fig. 4 clearly showed that the time courses of the fractional area change δ (due primarily to PGLa) and the rim intensity I (due to CF-PGLa) were essentially the same. Based on the interpretation A (i.e., the structural change model), we may infer that during the conversion from structure A to B, only CF-PGLa translocates from the external to the internal monolayer due to large structural fluctuation of lipid bilayers induced by the conversion of PGLa structure. Therefore, after the steady values of δ_1 and I_1 for an extended period, both the δ and the I started to increase simultaneously until new steady values of δ_2 and I_2 were achieved. In the interpretation A, we assume that the behavior of CF-PGLa in the membrane is different from that of PGLa. On the other hand, based on the interpretation B (i.e., the translocation model), the result of Fig. 4 indicated that the behavior of a low concentration of CF-PGLa in the membrane was the same as that of PGLa. The results shown in Figs. 2, 3, and 4 clearly indicated that high PGLa concentrations induced membrane permeation of AF647 via a two-step increase in δ and I; notably, the ratios of these values at the second steady state compared

19

to the first steady state (i.e., δ_2/δ_1 and I_2/I_1) approximated a value of 2. In the magainin 2-caused pore formation, a two-step grow in I was observed when pore formation started, along with an I_2/I_1 ratio of ~2 [35]. Those results were inferred to indicate the translocation of magainin 2 from the external to the internal leaflet, such that the same magainin 2 concentration, C, was attained in both leaflet [35]. If we consider that the binding of peptide in the membrane increases membrane area change and hence $\delta \propto C$, which was demonstrated experimentally for magainin 2 [35], we can infer that the fractional area change of the membrane where the peptide binds to both monolayers is twice that of the membrane where the peptide binds only to the outer monolayer. Therefore, based on the interpretation B we can conclude that PGLa (as well as CF-PGLa) transfers from the external leaflet to the internal leaflet before membrane permeation of AF-647 starts. Moreover, CF-PGLa entered the lumens of GUVs when CF-PGLa translocated across the bilayer, an event that occurred much before membrane permeation of AF-647. Irrespective of interpretation A and B, the results in this report indicated that CF-PGLa translocated across the lipid bilayer and then entered the GUV lumen.

Here, we consider the mechanism for the translocation of CF-PGLa and PGLa across the bilayer. In the interpretation A, CF-PGLa translocates from the external monolayer to the internal one during the conversion from structure A to B. The large structural change of PGLa may induce fluctuations of lipid bilayers, which may induce the translocation of CF-PGLa, although we do not know the details in the fluctuation of the bilayer. On the other hand, in the interpretation B, PGLa (as well as CF-PGLa) translocates from the external leaflet to the internal leaflet before membrane permeation of AF-647 starts. At present we have two hypotheses on the mechanism for the translocation of CF-PGLa and PGLa across the bilayer based on the interpretation B. One hypothesis (i.e., hypothesis I) is based on the supposition that the start of AF647 leakage is the same as the start of pore formation in the GUV membrane, which have been used in many researchers. Here, we consider a pore as a water hall in a bilayer with larger diameter than fluorescent dyes, and thus these dyes can pass through the pore. In this hypothesis I, we infer that PGLa (as well as CF-PGLa) transfers from the external leaflet to the internal leaflet before pore formation, and subsequently CF-PGLa entered the lumens of GUVs, which indicates that PGLa and CF-PGLa have an activity of cell-penetration as the CPPs, which can enter the cytosol of living

eukaryotic cells across their plasma membranes [40]. The other hypothesis (i.e., hypothesis II) is based on a following assumption. Before the start of AF647 leakage, a smaller pore may form in the lipid bilayer. Although AF647 cannot permeate through this smaller pore, PGLa (as well as CF-PGLa) can transfer from the external leaflet to the internal one through the pore. It is considered that peptides such as Bax-derived peptide and magainin 2 form toroidal pores at equilibrium [41-43], where the both leaflets bend and connect each other to form pore wall and hence the inner wall is comprised of hydrophilic segments of lipids and peptides. It is reported that some peptides rapidly translocated across the bilayer through these peptides-induced pores [34,35]. If we postulate that the initial structure of the PGLa-caused pore is also a toroidal one, PGLa (as well as CF-PGLa) can make lateral diffusion along this connected monolayer from the external monolayer to the internal one through the wall of the toroidal pore (i.e., translocate from the external leaflet to the internal one through the pore). After the translocation of PGLa (as well as CF-PGLa), the size of pore gradually increases and then AF647 leakage starts. The results of Fig. 1C, i.e., the membrane permeability coefficient of calcein, $P(t)$, increased with time before reaching a steady, maximum value of P^s, may support the hypothesis II.

If we consider that the hypothesis I is correct, CF-PGLa has an activity of cell-penetration as the CPPs. Here we compare the activities of cell-penetration and translocation across the bilayer of CF-PGLa (as well as PGLa) with those of typical CPPs such as transportan 10 (TP10) [33,34,45] and oligoarginine (R_9) [44]. The kinetics of the translocation of PGLa (as judged by the change in δ) and CF-PGLa (as judged by the change in I) differ from those of CF-TP10 and CF-R_9. For CF-TP10 and CF-R_9, the I gradually increased before reaching a steady value (i.e., a one-step increase), and for CF-TP10 the steady value of I did not change after pore formation. These results indicated that CF-TP10 and CF-R_9 molecules gradually translocated from the external leaflet to the internal one until their concentrations in both monolayers were saturated and that for CF-TP10 the surface concentration did not further increase even after pore formation (i.e., the symmetric transbilayer distribution of CF-TP10 induces pore formation). For CF-TP10, the time course of δ was similar to that of I [34]. In contrast, the results in this report (the two-step increase in δ and I) indicate that for high concentrations of PGLa and CF-PGLa, at the beginning of the interaction, these peptides stayed only in the outer leaflet for a long time before

suddenly starting to translocate from the external leaflet to the internal one, until the concentrations in the inner leaflet became the same as those in the outer leaflet. The translocation took a short time (i.e., 30−60 s; depending on the peptide concentration), suggesting cooperative behavior in the translocation of the peptide. In contrast, for lower concentrations of PGLa and CF-PGLa, the results (the one-step increase in δ and I) indicate that these peptides stayed only in the outer leaflet during the interaction and thus no AF647 leakage occurred. Moreover, the kinetics of the entering of CF-PGLa into the vesicle lumen also differed from that of CF-TP10 and CF-R$_9$. For example, CF-TP10 started to enter the GUV lumen after some lag time (30−200 s, depending on the conditions such as peptide concentration) following the transfer of peptides from the external to the internal leaflet [45]. The rates of entering of CF-TP10 and CF-R$_9$ into the lumen were small and hence the concentrations of these peptides in the GUV lumen after a short time interaction (6-10 min) were low. As a result, we could not observe a significant increase in lumen intensity due to these peptides. To detect the entering of these peptides into the lumen, we applied a special method using GUVs containing small GUVs and GUVs containing LUVs [33,34,44,45]. On the other hand, CF-PGLa started to enter the GUV lumen immediately after the transfer of CF-PGLa from the external leaflet to the internal leaflet. We may attribute this great difference to the larger value of the rate constant of unbinding of CF-PGLa from the inner leaflet into the lumen adjacent to the membrane, k_{OFF}, compared with those of CF-TP10 and CF-R$_9$ [33,44]. Moreover, the rate of entering of CF-PGLa into the lumen is so large that we observed a large grow in lumen intensity due to CF-PGLa at 6 min of interaction.

If CF-PGLa (as well as PGLa) has an activity of cell-penetration as the CPPs, what kind of mechanism for the translocation of CF-PGLa (as well as PGLa) can we consider? There are several models on the mechanism of the transfer of CPPs across lipid bilayers. In the first model, the transbilayer movement of CPPs occurs through CPP-caused pores in the bilayer [46-48]. In the second model, the transfer of CPPs occurs through inverted micelles in the bilayer, such that, during the transfer, the CPPs bind with negatively charged lipids with a defined stoichiometry to form the inverted micelles [49-51]. In the third model, the transbilayer movement of CPPs proceeds through transient hydrophilic pre-pores in the bilayer [34,44,45]. In the L_α phase, the thermal

fluctuation of the structure of the lipid bilayers is large, which induces transient reduction in the lipid lateral density at some local areas in the bilayer [52-55]. One class of an area of reduced density is called the hydrophilic pre-pore, which consists of a toroidal structure (i.e., lipid headgroups face with water at the wall of the pre-pore) [52-55]. The thermal fluctuation of the radius of the pre-pore, r, can be considered based on the theory of tension-caused pore formation [52-54]. The formation of a pre-pore in the bilayer alters the total free energy of the membrane by a free energy term, $U(r)$ (called the free energy of a pre-pore). One of the term of $U(r)$ is $-\pi r^2 \sigma$ (where σ is the lateral tension in the bilayer), which is due to a decrease in elastic energy. The other term of $U(r)$ is $2\pi r \Gamma$ (where Γ is line tension). Therefore,

$$U(r) = 2\pi r \Gamma - \pi r^2 \sigma \qquad (3).$$

The maximum of $U(r)$ is $U_{max} = U(r_c) = \pi \Gamma^2 / \sigma$ at $r = r_c$ ($= \Gamma / \sigma$), which can be considered as the activation energy of the tension-caused pore formation. When the radius of a pre-pore is smaller than the critical radius, r_c, the pre-pore closes rapidly. After a long thermal fluctuation, when the radius reaches r_c, the pre-pore is converted into a pore. This theory has been successfully applied to several phenomena (e.g., the closure dynamics of tension-induced pores [25,56] and the rate constant of tension-caused pore formation [53,57,58]). The initial slope of $U(r)$ diminishes with a reduction in U_{max}, such that the frequency of pre-pore formation grows with an increase in tension [34]. This effect enhances the rate of translocation of CPPs. On the basis of the third model, we consider a mechanism for the translocation of PGLa across the bilayer as follows. As indicated in Fig. 2D, at and above 1.2 μM PGLa, δ in the 1st steady state was essentially constant, indicating that the tension due to this stretching is the same. This observation means that the frequency of pre-pore formation induced by tension remains the same. However, the rate of PGLa-caused pore formation greatly depended on the PGLa concentration; no pore formation occurred for 6 min at 1.2 μM PGLa (Fig. 2A), pore formation occurred in 40% of the examined GUVs at 2.9 μM PGLa (Fig. 2C), and pore formation occurred in 100% of the examined GUVs at 5.8 μM PGLa (Fig. 2B). Therefore, the simple third model cannot explain the translocation of PGLa. As described above, PGLa exists in the S-state at low PGLa concentration, and it exists in the T-state at higher PGLa concentrations [13-15,59]. Based on the interpretation B, the increase in the

fraction of the T-state of PGLa may play a key role in its translocation of PGLa across the bilayer, although we have no direct evidence for this hypothesis. One of the characteristics of PGLa-induced translocation across the bilayer is that the translocation of PGLa began after the peptide had been present in the external monolayer for an extended time (20–260 s). This long interval may be required for the conformational change of PGLa from the S-state to the T-state. The T-state may be required for the translocation of PGLa across the bilayer.

Recently, a MD simulation of the interactions of PGLa with lipid bilayers has been reported [60], indicating that PGLa can transfer across lipid bilayers without pore formation. This result supports the interpretation B and hypothesis I in the present report. According to Ulmschneider's MD simulations [60], the interaction of two or three peptides induces a transient (μs-order) transmembrane orientation of a PGLa molecule, permitting a PGLa molecule to translocate from one monolayer to the other. The conditions of the MD simulations (including temperatures of 120–180 °C and an ion concentration of 0.1 M NaCl) differed from the experimental conditions (25 °C and 0.15 M NaCl) used in the current report, making it difficult to quantitatively compare the MD simulations with our own results. For example, the large lag time from the state A (i.e., CF-PGLa molecules locate only in the outer monolayer) to the translocation of the peptides across the bilayer observed in our experiments cannot be explained by the MD simulation results. Further experiments under various conditions will be necessary to compare these experimental results with those of the MD simulations.

5. CONCLUSION

We found that PGLa induced pores in single PG/PC (4/6)-GUVs and that the rate of PGLa-caused pore formation was raised as PGLa concentration increased. Membrane permeability coefficient of calcein increased with time to reach a steady value, which continued for an extended time. These results clearly indicate that PGLa forms pores in the PG/PC (4/6) membrane for an extended time. At high PGLa concentrations, the time course of the CF-PGLa surface concentration in the GUV membrane, C_M, judged by the rim intensity, showed a two-step increase, and the ratio of concentration at the second steady state to that at the first steady state (C_M (S2)/ C_M (S1) = I_2/I_1) was almost 2, and I_{lumen} due to CF-PGLa started to increase rapidly when C_M began to

grow from the first constant value, C_M (S1). In the interaction of 100% CF-PGLa with PG/PC (4/6)-GUVs, the similar results were observed (S.2. and Fig. S2 in the SI). These results indicate that CF-PGLa translocated from the external leaflet to the internal one before membrane permeation of AF647, i.e., pore formation, and CF-PGLa started to enter the GUV lumen immediately after the translocation of CF-PGLa across the bilayer began. On the other hand, the time course of the fractional area change, δ, showed a two-step increase at high PGLa concentrations, and δ_2/δ_1 was almost 2. If we assume that the behavior of low concentration of CF-PGLa is the same as that of PGLa, these results can be explained by considering two processes that are the structural change of PGLa and the translocation of PGLa from the external leaflet to the internal leaflet. In the first stage, PGLa binds to the external leaflet as S-state until first steady state. At the next extended state, some of the S-states change to T-states which lead the translocation of PGLa from the external to the internal leaflet and simultaneously the PGLa binds to external leaflet from aqueous solution to increase C_M and δ values again until second steady state. As soon as PGLa is translocated, the internal leaflet releases PGLa to the GUV lumen. It is assumed that the structural change of PGLa from S-state to T-state may not vary δ values but increase of PGLa concentration causes the increment of δ values. Consequently, PGLa peptides with T-state distribute to both leaflets to start forming pores in the membrane to show permeability. On the other hand, if we assume that the behavior of CF-PGLa is different from that of PGLa, these results can be explained as follows. In the first stage, PGLa binds to the external leaflet as S-state, and after an extended time some of the S-states change to T-states, which increases δ values again until second steady state. Then after some time pore formation starts to occur. Consequently, PGLa peptides locate only in the outer leaflet before pore formation. In conclusion, in this report we elucidated several elementary processes on the PGLa-induced pore formation, which would contribute to reveal the mechanism for the PGLa-induced pore formation in near future.

Supporting Information:

Data of the relationship between the location of 100% CF-PGLa and the AF647 leakage, and the experimental method to determine the PGLa concentration near single GUVs.

References

[1] Zasloff, M. (2002) Antimicrobial peptides of multicellular organisms, *Nature 415*, 389-395.

[2] Melo, M. N., Ferre, R., and Castanho, A. R. B. (2009) Antimicrobial peptides: linking partition, activity and high membrane-bound concentrations, *Nat. Rev. Microbiol. 8,* 1-5.

[3] Propheter, D. C., Chara, A. L., Harris, T. A., Ruhn, K. A., and Hooper L. V. (2017) Resistin-like molecule β is a bactericidal protein that promotes spatial segregation of the microbiota and the colonic epithelium, *Proc. Natl. Acad. Sci. USA*. 114, 11027-11033.

[4] Sochacki, K. A., Barns, K. J., Bucki, R., and Weisshaar, J. C. (2011) Real-time attack on single Escherichia coli cells by the human antimicrobial peptide LL-37, *Proc. Natl. Acad. Sci. USA. 108*, E77-E81.

[5] Park, C. B., Yi, K.-S., Matsuzaki, K., Kim, M. S., and Kim, S. C. (2000) Structure-activity analysis of buforin II, a histone H2A-derived antimicrobial peptide: The proline hinge is responsible for the cell-penetrating ability of buforin II, *Proc. Natl. Acad. Sci. USA. 97*, 8245-8250.

[6] Moniruzzaman, M., Islam, M. Z., Dohra, H., and Yamazaki, M. (2017) Entry of a Six-Residue Antimicrobial Peptide Derived from Lactoferricin B into Single Vesicles and *Escherichia coli* without Damaging their Membranes, *Biochemistry 56*, 4419-4431.

[7]   Hoffmann, W., Richter, K., and Kreil, G. (1983) A novel peptide designated PYL[a] and its precursor as predicted from cloned mRNA of *Xenopus laevis* skin, *EMBO J. 2*, 711-714.

[8] Giovannini, M. G., Poulter, L., Gibson, B. W., and Williams, D. H. (1987) Biosynthesis and degradation of peptides derived from Xenopus laevis prohormones, *Biochem. J. 243*, 113-120.

[9] Zasloff, M., Martin, B., and Chen, H.-C. (1988) Antimicrobial activity of synthetic magainin peptides and several analogues, *Proc. Natl. Acad. Sci. USA. 85*, 910-913.

[10] Soravia, E., Martini, G., and Zasloff, M. (1988) Antimicrobial properties of peptides from Xenopus granular gland secretions, *FEBS Lett. 228*, 337-340.

[11] Latal, A., Degovics, G., Epand, R. F., Epand, R. M., and Lohner, K. (1997) Structural aspects of the interaction of peptidyl-glycylleucine-carboxyamide, a highly potent antimicrobial peptide from frog skin, with lipids, *Eur. J. Biochem. 248*, 938-946.

[12] Wieprecht, T., Apostolov, O., Beyermann, M., and Seelig, J. (2000) Membrane binding and pore formation of the antibacterial peptide PGLa; thermodynamic and mechanistic aspects, *Biochemistry 39*, 442-452.

[13] Bechinger, B., Zasloff, M., and Opella, S. J. (1998) Structure and dynamics of the antibiotic peptide PGLa in membranes by solution and solid-state nuclear magnetic resonance spectroscopy, *Biophys. J. 74*, 981-987.

[14] Glaser, R. W., Sachse, C., Dürr, U. H. N., Wadhwani, P., Afonin, S., Strandberg, E., and Ulrich, A. S. (2005) Concentration-dependent realignment of the antimicrobial peptide PGLa in lipid membranes observed by solid-state ^{19}F-NMR, *Biophys. J. 88*, 3392-3397.

[15] Tremouihac, P., Strandberg, E., Wadhwani, P., and Ulrich, A. S. (2006) Conditions affecting the re-alignment of the antimicrobial peptide PGLa in membranes as monitored by solid state ^{2}H-NMR, *Biochim. Biophys. Acta, 1758*, 1330-1342.

[16] Williams, R. W., Starman, R., Taylor, K. M., P., Gable, K., Beeler, T., Zasloff, M., and Covell, D. (1990) Raman spectroscopy of synthetic antimicrobial frog peptides magainin 2a and PGLa, *Biochemistry 29*, 4490-4496.

[17] Vaz Gomes, A., de Waal, A., Berden, J. A., and Westerhoff, H. V. (1993) Electric potentiation, cooperativity, and synergism of magainin peptides in protein-free liposomes, *Biochemistry 32*, 5365-5372.

[18] Matsuzaki, K., Mitani, Y., Akada, K., Murase, O., Yoneyama, S., Zasloff, M., and Miyajima, K. (1998) Mechanism of synergism between antimicrobial peptides magainin 2 and PGLa, *Biochemistry 37*, 15144-15153.

[19] Blazyk, J., Wiegand, R., Klein, J., Hammer, J., Epand, R. M., Epand, R. F., Maloy, W. L., and Kari, U. PO. (2001) A novel linear amphipathic β-sheet cationic antimicrobial peptide with enhanced selectivity for bacterial lipids, *J. Biol. Chem. 276*, 27899-27906.

[20] Westerhoff, H. V., Zasloff, M., Rosner, J. L., Hendler, R. W., de Waal, A., Vaz Gommes, A., Jongsma, A. P. M., Riethorst, A., and Juretic, D. (1995) Functional synergism of the magainins PGLa and magainin-2 in Escherichia coli, tumor cells and liposomes, *Eur. J. Biochem. 228*, 257-264.

[21] Tremouilhac, P., Strandberg, E., Wadhwani, P., and Ulrich, A. S. (2006) Synergistic transmembrane alignment of the antimicrobial heterodimer PGLa/magainin 2, *J. Biol. Chem. 281*, 32089-32094.

[22] Sainikov, E. S., and Bechinger, B. (2011) Lipid-controlled peptide topology and interactions in bilayers: structural insights into the synergistic enhancement of the antimicrobial activities of PGLa and magainin 2, *Biophys. J*. 100, 1473-1480.

[23] Strandberg, E., Hom, D., Reisser, S., Zweweck, J., Wadhwani, P., and Ulrich, A. S. (2016) ^{2}H-NMR and MD simulations reveal membrane-bound condition of magainin 2 and its synergy with PGLa, *Biophys. J., 111*, 2149-2161.

[24] Yamazaki, M. (2008) The single GUV method to reveal elementary processes of leakage of internal contents from liposomes induced by antimicrobial substances, *Adv. Planar Lipid Bilayers and Liposomes 7*, 121-142.

[25] Sandre, O., Moreaux, L., and Brochard-Wyard, F. (1999) Dynamics of transient pores in stretched vesicles, *Proc. Natl. Acad. Sci. USA. 96*, 10591-10596.

[26] Rawictz, W., Olbrich, K. C., McIntosh, T., Needham, D., and Evans, E. (2000) Effect of chain length and unsaturation on elasticity of lipid bilayers, *Biophys. J. 79*, 328-339.

[27] Farge, E., and Devaux, P. F. (1992) Shape changes of giant liposomes induced by an asymmetric transmembrane distribution of phospholipids, *Biophys. J. 61*, 347-357.

[28] Baumgart, T., Hess, S. T., and Webb, W. W. (2003) Imaging coexisting fluid domains in biomembrane models coupling curvature and line tension, *Nature 425*, 821-824.

[29] Islam, M. Z., Alam, J. M., Tamba, Y., Karal, M. A. S., and Yamazaki, M. (2014) The single GUV method for revealing the functions of antimicrobial, pore-forming toxin, and cell-penetrating peptides or proteins, *Phys. Chem. Chem. Phys. 16*, 15752-15767.

[30] Tamba, Y., and Yamazaki, M. (2005) Single giant unilamellar vesicle method reveals effect of antimicrobial peptide Magainin 2 on membrane permeability, *Biochemistry 44*, 15823-15833.

[31] Tamba, Y., and Yamazaki, M. (2009) Magainin 2-induced pore formation in membrane depends on its concentration in membrane interface, *J. Phys. Chem. B 113*, 4846-4852.

[32] Tamba, Y., Ariyama, H., Levadny, V., and Yamazaki, M. (2010) Kinetic pathway of antimicrobial peptide magainin 2-induced pore formation in lipid membranes, *J. Phys. Chem. B 114*, 12018-12026.

[33] Islam, M. Z., Ariyama, H., Alam, J. M., and Yamazaki, M. (2014) Entry of cell-penetrating peptide transportan 10 into a single vesicle by translocating across lipid membrane and its induced pores, *Biochemistry 53*, 386-396.

[34] Islam, M. Z., Sharmin, S., Levadnyy, V., Shibly, S. U. A., and Yamazaki, M. (2017) Effects of mechanical properties of lipid bilayers on the entry of cell-penetrating peptides into single vesicles, *Langmuir, 33*, 2433-2443.

[35] Karal, M. A. S., Alam, J. M., Takahashi, T., Levadny, V., and Yamazaki, M. (2015) Stretch-Activated Pore of Antimicrobial Peptide Magainin 2, *Langmuir 31*, 3391-3401.

[36] Hasan, M., Karal, M. A. S., Levadnyy, V., and Yamazaki, M. (2018) Mechanism of initial stage of pore formation induced by antimicrobial peptide magainin 2, *Langmuir* **34**, 3349-3362.

[37] Tamba, Y., Terashima, H., and Yamazaki, M. (2011) A membrane filtering method for the purification of giant unilamellar vesicles, *Chem. Phys. Lipids 164*, 351-358.

[38] Alam, J. M., Kobayashi, T., and Yamazaki, M. (2012) The Single Giant Unilamellar Vesicle Method Reveals Lysenin-Induced Pore Formation in Lipid Membranes Containing Sphingomyelin, *Biochemistry 51*, 5160-5172.

[39] Jung, C., Lee, J., Kang, M., and Kim, S. W. (2014) Measurement of the temperature-dependent diffusion properties of nanoparticles by using fluorescence correlation spectroscopy, *J. Korean Phys. Soc. 65*, 1083-1089.

[40] Islam, M. Z., Sharmin, S., Moniruzzaman, M., and Yamazaki, M. (2018) Elementary Processes for the Entry of Cell-Penetrating Peptides into Lipid Bilayer Vesicles and Bacterial Cells, *Appl. Microbiol. Biotechnol. 102*, 3879-3892.

[41] Matsuzaki, K., Murase, O., Fujii, N., and Miyajima, K. (1996) An antimicrobial peptide, magainin 2, induced rapid flip-flop of phospholipids coupled with pore formation and peptide translocation, *Biochemistry 35*, 11361-11368.

[42] Ludtke, S. J., He, K., Heller, K. H., Harroun, T. A., Yang, L., and Huang, H. W. (1996) Membrane pores induced by magainin, *Biochemistry 35*, 13723-13728.

[43] Yang, L. T., Weiss, M., Lehrer, R. I., and Huang, H. W. (2000) Crystallization of antimicrobial pores in membranes: magainin and protegrin, *Biophys. J. 79*, 2002-2009.

[44] Sharmin, S., Islam, M. Z., Karal, M. A. S., Shibly, S. U. A., Dohra, H., and Yamazaki, M. (2016) Effects of lipid composition on the entry of cell-penetrating peptide oligoarginine into single vesicles, *Biochemistry 55*, 4154-4165.

[45] Moghal, M. M. R., Islam, M. Z., Sharmin, S., Levadnyy, V., Moniruzzaman, M., and Yamazaki, M. (2018) Continuous detection of entry of cell-penetrating peptide transportan 10 into single vesicles, *Chem. Phys. Lipids, 212*, 120-129.

[46] Mishra, A., Gordon, V. D., Yang, L., Coridan, R., and Wong, G. C. L. (2008) HIV TAT forms pores in membranes by inducing saddle-spray curvature: potential role of bidentate hydrogen bonding, *Angew. Chem. Int. Ed. 47*, 2986-2989.

[47] Ciobanasu, C., Siebrasse, J. P., and Kubitscheck, U. (2010) Cell-penetrating HIV1 TAT peptides can generate pores in model membranes, *Biophys. J. 99*, 153-162.

[48] Mishra, A., Lai, G. H., Schmidt, N. W., Sun, V. Z., Rodriguez, A. R., Tong, R., Tang, L., Cheng, J., Deming, T. J., Kamei, D. T., and Wong, G. C. L. (2011) Translocation of HIV TAT peptide and analogues induced by multiplexed membrane and cytoskeletal interactions, *Proc. Natl. Acad. Sci. USA, 108,* 16883-16888.

[49] Berlose, J.-P., Convert, O., Derossi, D., Brunissen, A., and Chassaing, G. (1996) Conformational and associative behaviours of the third helix of antennapedia homeodomain in membrane-mimetic environments, *Eur. J. Biochem. 242*, 372-386.

[50] Kawamoto, S., Takasu, M., Miyakawa, T., Morikawa, R., Oda, T., Futaki, S., and Nagao, H. (2011) Inverted micelles formation of cell-penetrating peptide studied by coarse-grained simulation: Importance of attractive force between cell-penetrating peptides and lipid head group, *J. Chem. Phys. 134*, 095103.

[51] Swiecicki, J. -M., Bartsch, A., Tailhades, J., Di Pisa, M., Heller, B., Chassaing, G., Mansuy, C., Burlina, F., and Lavielle, S. (2014) The efficacies of cell-penetrating peptides in accumulating in large unilamellar vesicles depend on their ability to form inverted micelles, *Chem. Bio. Chem. 15*, 884-891.

[52] Glaser, R. W., Leikin, S. L., Chernomordik, L. V., Pastushenko, V. F., and Sokirko, A. I. (1988) Reversible electrical breakdown of lipid bilayers: formation and evolution of pores, *Biochim. Biophys. Acta 940*, 275-287.

[53] Evans, E., Heinrich, V., Ludwig, F., and Rawicz, W. (2003) Dynamic tension spectroscopy and strength of biomembranes, *Biophys. J. 85*, 2342-2350.

[54] Fuertes, G. , Giménez, D. , Esteban-Martín, S, , Sánchez-Muñoz, O. L. , and Salgado, J. (2011) A lipocentric view of peptide-induced pores, *Eur. Biophys. J. 40*, 399-415.

[55] Akimov, S. A., Volynsky, P. E., Galimzyanov, T. R., Kuzmin, P. I., Pavlov, K. V., Batishchev, O. V. (2017) Pore formation in lipid membrane I: Continuous reversible trajectory from intact bilayer through hydrophobic defect to transversal pore, *Sci. Rep. 7*, 12152.

[56] Karatekin, E., Sandre, O., Guitouni, H., Borghi, N., Puech, P. –H., and Brochard-Wyart, F. (2003) Cascades of transient pores in giant vesicles: line tension and transport, *Biophys. J. 84*, 1734-1749.

[57] Levadny, V., Tsuboi, T., Belaya, M., and Yamazaki, M. (2013) Rate Constant of Tension-Induced Pore Formation in Lipid Membranes, *Langmuir*, *29*, 3848-3852.

[58] Evans, E., and Smith, B. A. (2011) Kinetics of hole nucleation in biomembrane rupture, *New J. Phys.13*, 095010.

[59] Strandberg, E., Tremouihac, P., Wadhwani, P., and Ulrich, A. S. (2009) Synergetic transmembrane insertion of the heterodimeric PGLa/magainin 2 complex studied by solid-state NMR, *Biochim. Biophys. Acta, 1788*, 1667-1679.

[60] Ulmschneider, J. P. (2017) Charged antimicrobial peptides can translocate across membranes without forming channel-like pores, *Biophys. J. 113*, 73-81.